

Manuscript Number: JALCOM-D-15-08501R2

Title: Which wets  $TiB_2$  inoculant particles: Al or  $Al_3Ti$ ?

Article Type: Full Length Article

Keywords: Interfacial energy; Density functional theory; Nucleation; Aluminium;  $Al_3Ti$ ;  $TiB_2$

Corresponding Author: Dr. Andrew Horsfield,

Corresponding Author's Institution:

First Author: David Wearing, PhD

Order of Authors: David Wearing, PhD; Andrew Horsfield; Wenwu Xu, PhD; Peter D Lee, PhD

Abstract: Abstract  $TiB_2$  particles are proven effective nucleants of commercial purity aluminium, resulting in smaller grains and hence greater desired mechanical properties; however, there is uncertainty as to the mechanism by which it operates. Here we clarify what happens in the initial stages by computing the total Gibbs energy change associated with four possible nucleation mechanisms, each characterised by the termination of the  $TiB_2(0001)$  substrate (Ti or B) and the solid that forms on it (Al or  $Al_3Ti$ ). The appropriate solid//solid interfacial energies are derived from Density Functional Theory (DFT) calculations, while the bulk energies are derived from thermodynamic data, supplemented with strain energies calculated from DFT. Solid//liquid interfacial energies are estimated using simple models with parameters based on the literature and DFT calculations. The results suggest that the Ti termination of  $TiB_2$  is more stable than the B termination in the melt, and that the direct formation of Al off a Ti-terminated  $TiB_2$  substrate is the most favourable mechanism for the nucleation of Al rather than the previously proposed formation of a  $Al_3Ti$  interlayer. On the B termination of  $TiB_2$ , Al formation is more stable for thick solid layers, but this is much more uncertain for thin solid layers where it is possible that  $Al_3Ti$  formation is more stable.

*Journal of Alloys and Compounds*

Editor Office

Dr. Andrew Horsfield  
Department of Materials  
Imperial College London,  
South Kensington Campus  
London SW7 2AZ, UK  
Tel. : +44 (0)20 7594 6753  
E-mail: [a.horsfield@imperial.ac.uk](mailto:a.horsfield@imperial.ac.uk)

London, October 26, 2015

Dear Editor,

Please find attached our manuscript entitled “Which wets  $\text{TiB}_2$  inoculant particles: Al or  $\text{Al}_3\text{Ti}$ ?” which we hope you will consider for publication in *Journal of Alloys and Compounds*.

Using first principle calculations, Gibbs bulk energy literature data and thermodynamic arguments, we quantitatively compare four hypothetical mechanisms for the nucleation of aluminium. The four mechanisms involve one of two substrates, B or Ti terminated  $\text{TiB}_2(0001)$ , in an Al melt with some dissolved Ti, from which one solid, either strained Al(111) or  $\text{Al}_3\text{Ti}(112)$ , nucleates, forming a solid/solid interface. We conclude that under typical industrial conditions, strained Al formation on a Ti terminated  $\text{TiB}_2$  substrate is the most stable mechanism of the four compared here. The results of this study are important for the ongoing debate surrounding the nucleation of CP aluminium.

We hope you will find the paper suitable for publication in *Journal of Alloys and Compounds*.

Sincerely yours,

Andrew Horsfield

**Prime Novelty Statement:**

This is the first microscopic thermodynamic analysis of the nucleation of solid commercial purity Al off the widely used refiner  $\text{TiB}_2$  that includes all important contributions. We bring new clarity to the debate over the nucleation mechanism. Our results suggest that the Ti termination of  $\text{TiB}_2$  is more stable than the B termination in the Al melt, and that the direct formation of Al off a Ti-terminated  $\text{TiB}_2$  substrate is more stable than  $\text{Al}_3\text{Ti}$  formation. On the B termination of  $\text{TiB}_2$ , Al formation is more stable for thick solid layers, but this is much more uncertain for thin solid layers where it is possible that  $\text{Al}_3\text{Ti}$  formation is more stable.

We thank the referees for their careful reading of our manuscript, and for the insightful comments and suggestions provided. We have carefully addressed all of the suggestions made, and our responses are given below. Text in italics is a comment from a referee, which is then followed by our response in normal text.

### Referee 1

*1. In the abstract and the first paragraph it is said that we grain refine Al alloys to improve the properties. I don't think that this is actually the case. Practically processing improvements are more beneficial, e.g. reduced hot tearing.*

We have changed 'greater strength' to 'improved mechanical properties' in the abstract; I've changed the second line of the introduction to include further details of these improvements, including hot tearing. New references have been added accordingly:

“... with smaller equiaxed grains generally leading to greater desirable properties such as improved yield strength and toughness due to the Hall-Petch effect [1,2], together with reduced defects such as porosity [3] and hot tearing [4].”

*2. line 228 needs units for the interfacial energies*

Done, see revised paper.

*3. The captions in Figs 7 and 8 seem to suggest that there are multiple graphs. I suggest replacing the word 'each' with 'the'*

Done, see revised paper.

*4. There have also been a number of publications around epitaxial growth theories of nucleation. It would be interesting to know how the authors see their findings fitting in with those approaches. It may not be the appropriate place to mention them here, but I suspect a reference to them may provide more context to the work presented here.*

We have included two sentences at the beginning of section 2 (modelling the nucleation of aluminium) that refer the reader to appropriate journal citations and a recent book on nucleation by Kelton and Greer which provides a great overview of the suggested theories.

## Referee 2

(1) *The authors tried to demonstrate that the strained Al at the interface with TiB<sub>2</sub> may be the nuclei. They argued that the thin layers observed by Schumacher et al. could be strained Al with the same interplanar separation as Al<sub>3</sub>Ti. However, a recent paper reported that a Ti-rich monolayer exists on the TiB<sub>2</sub> surface, and it is most likely to be a (112) Al<sub>3</sub>Ti two-dimensional (2D) compound. (Z. Fan et al., Acta Mater. 84 (2015) 292).*

See revised paper: Introduction, 3<sup>rd</sup> paragraph and first 2 lines of the 4<sup>th</sup> paragraph. It now reads

“Other experiments showed that, in addition to TiB<sub>2</sub> particles, excess solute titanium in the melt was also needed for  $\alpha$ -Al nucleation to occur [8]. The role played by this excess Ti is not yet completely understood, but it is thought that in addition to acting as a diffusion restrictor [9], Ti is needed to form Al<sub>3</sub>Ti which nucleates off the TiB<sub>2</sub> forming a thin layer; Al then nucleates off the Al<sub>3</sub>Ti layer [1]. The confidence in this Al<sub>3</sub>Ti nucleation hypothesis is based on Schumacher’s TEM experiments [2, 3, 4, 5, 6, 7], backed up by more recent TEM experiments by Fan [10], and by in situ synchrotron X-ray diffraction experiments [11], where diffraction peaks corresponding to plane separations similar to the those of bulk Al<sub>3</sub>Ti were observed at the onset of aluminium solidification.

However, none of these experimental results are able to show the precise chemical composition of the nucleating layer. It is possible that what is being observed in these experiments is actually strained  $\alpha$ -Al, as suggested by Wang et al. [12], who proposed that the thin layers observed by Schumacher et al. [5] could be strained Al with the same interplanar separation as Al<sub>3</sub>Ti. If this is the true mechanism, then the role of the excess Ti could be to ensure that TiB<sub>2</sub> particles become Ti-terminated.”

(2) *This study reveals that a thin layer of strained Al at the interface of TiB<sub>2</sub> in the CP-Al melt is more stable than strained Al<sub>3</sub>Ti, due to the contribution of the large strain energy from the strained Al<sub>3</sub>Ti, where the strain energy is calculated with the DFT at a ground state. However, it is quite susceptible to extrapolate the data at 0 K to above the melting point, as the authors admitted. The misfit (0.09%) of Al<sub>3</sub>Ti/TiB<sub>2</sub> is much smaller than that (-4.22%) of Al/TiB<sub>2</sub> at the melting point of Al, due to the different thermal expansion coefficient for Al and Al<sub>3</sub>Ti. Thus, the strain energy of Al<sub>3</sub>Ti/TiB<sub>2</sub> is not necessarily larger than that of Al/TiB<sub>2</sub> at the melting point.*

This is an important point and we have fully considered it. We have checked the effect of thermal expansion, and it is predicted to not significantly affect our main results. Our calculations predict that at 0K and at the Al melting point, both Al(111) and Al<sub>3</sub>Ti(112) will have to stretch to accommodate TiB<sub>2</sub>(0001), but that Al<sub>3</sub>Ti(112) will still have to stretch more than Al(111) at both temperatures. Furthermore, thermal expansion effects seem to further favour Al as the nucleation solid. We have added material to and edited the last paragraph of section 4.4 (page 9) to show this point. Below is the more detailed workings out:

Going from 0K to 933K, the 'a' parameter of TiB<sub>2</sub> will go from **3.025 to 3.043**, an increase of **0.6%** (Munro, *Material Properties of Titanium Diboride*, Journal of Research of NIST, Vol 105, 5, Sep–Oct 2000).

The thermal expansion of Al at 298K is about  $22 \times 10^{-6}$  m/(m K) (Nix, F. C. and MacNair, D., *The Thermal Expansion of Pure Metals: Copper, Gold, Aluminum, Nickel, and Iron*, *Phys. Rev.* (1941), 597-605.). Taking this as an average value from 0K to 933K means the 'a' parameter in the Al(111) plane will go from about **2.86 to 2.92**, an increase of 2.1% (take 'a' of the unit cell and divide by  $\sqrt{2}$ );

The unstrained DO<sub>22</sub> Al<sub>3</sub>Ti(112) plane is slightly asymmetrical, so the plane has two separation distances between nearest atoms, from our 0K results they are **2.72** and **2.89** (calculated thusly:  $a/\sqrt{2}$ , and  $\sqrt{(c^2/16 + a^2/4)}$ , where 'a' and 'c' are the unit cell parameters).

Using our 0K Al<sub>3</sub>Ti results along with the results of a recent paper (Saumitra Saha, *Temperature dependent lattice misfit and coherency of Al<sub>3</sub>X (X = Sc, Zr, Ti and Nb) particles in an Al matrix*, *Acta Materialia* 89 (2015) 109–115) that contains calculations of the relative misfit of Al and Al<sub>3</sub>Ti from 0K to 800K, we calculate that the two nearest-atom separations in the Al<sub>3</sub>Ti(112) plane at 933K will be about **2.75** and **2.91**, increases of 1.1% and 0.7% from the 0K separations.

Hence according to these separations, from 0K to 933K, the TiB<sub>2</sub>//Al(111) strain goes from about +5.5% to +4.2%; likewise the TiB<sub>2</sub>//Al<sub>3</sub>Ti(112) strain for the two separations goes from +11.2% to +10.7% and +4.7% to +4.6%. Hence, we calculate that it is Al(111) that reduces its strain more than Al<sub>3</sub>Ti(112), over the temperature increase. This should result in a reduced strain of TiB<sub>2</sub>//Al over TiB<sub>2</sub>//Al<sub>3</sub>Ti(112).

(3) Eq. (3)  $\langle \gamma \rangle_{\text{sub/melt}} = \langle \gamma \rangle_{\text{sub/vac}} + \langle \gamma \rangle_{\text{melt/vac}} + \langle \Delta \rangle$   
 $\langle \gamma \rangle_{\text{sub/melt}}$  might be equivalent to the Yong' equation  $\langle \gamma \rangle_{\text{sub/melt}} = \langle \gamma \rangle_{\text{sub/vac}} - \langle \gamma \rangle_{\text{melt/vac}} \cdot \cos \langle \alpha \rangle$ , where  $\langle \alpha \rangle$  is contact angle. It may become  $\langle \gamma \rangle_{\text{sub/melt}} = \langle \gamma \rangle_{\text{sub/vac}} - \langle \gamma \rangle_{\text{melt/vac}}$  while completely wet and  $\langle \alpha \rangle = 0$ . The two equations appear to be inconsistent if considering the contribution of  $\langle \gamma \rangle_{\text{melt/vac}}$ .

We believe that the Young's equation is not applicable in our situation as we have complete wetting. Furthermore, the  $\langle \gamma \rangle_{\text{melt/vac}}$ ,  $\langle \gamma \rangle_{\text{sub/vac}}$  and  $\langle \gamma \rangle_{\text{sub/melt}}$  are not in equilibrium with each other in our equation, whereas they are in Young's equation. Young's equation is derived for perfectly flat and rigid substrates that are large enough to accommodate the (non-wetting) liquid at its ideal equilibrium wetting angle (such as a drop of water on a lotus leaf).

(4) In Fig. 1 & 2, the interfacial energy  $\langle \gamma \rangle$  becomes negative for some Ti chemical potentials  $\mu_{\text{Ti}}$ , which seems unphysical.

This is indeed unphysical, as a negative gamma means that surfaces form spontaneously. We have retained the negative values to help the reader fully see and compare each plot. We have added a comment to the text explaining this on page 11.

(5) *In Fig. 4, the curve  $TiB_2(B)//Al_3Ti//melt$  is missing.*

While the line was not missing, it was hard to see, as it was overlapping with another one. It has now been made clearer.

## Which wets $\text{TiB}_2$ inoculant particles: Al or $\text{Al}_3\text{Ti}$ ?

David Wearing<sup>a</sup>, Andrew P. Horsfield<sup>a</sup>, Wenwu Xu<sup>b,c</sup>, Peter D. Lee<sup>b,c</sup>

<sup>a</sup>*Department of Materials, Imperial College London, Prince Consort Road, London, SW7 2BP, UK*

<sup>b</sup>*School of Materials, The University of Manchester, Oxford Rd., M13 9PL, UK*

<sup>c</sup>*Research Complex at Harwell, Didcot OX11 0FA, UK*

---

### Abstract

$\text{TiB}_2$  particles are proven effective nucleants of commercial purity aluminium, resulting in smaller grains and hence greater desired mechanical properties; however, there is uncertainty as to the mechanism by which it operates. Here we clarify what happens in the initial stages by computing the total Gibbs energy change associated with four possible nucleation mechanisms, each characterised by the termination of the  $\text{TiB}_2(0001)$  substrate (Ti or B) and the solid that forms on it (Al or  $\text{Al}_3\text{Ti}$ ). The appropriate solid//solid interfacial energies are derived from Density Functional Theory (DFT) calculations, while the bulk energies are derived from thermodynamic data, supplemented with strain energies calculated from DFT. Solid//liquid interfacial energies are estimated using simple models with parameters based on the literature and DFT calculations. The results suggest that the Ti termination of  $\text{TiB}_2$  is more stable than the B termination in the melt, and that the direct formation of Al off a Ti-terminated  $\text{TiB}_2$  substrate is the most favourable mechanism for the nucleation of Al rather than the previously proposed formation of a  $\text{Al}_3\text{Ti}$  interlayer. On the B termination of  $\text{TiB}_2$ , Al formation is more stable for thick solid layers, but this is much more uncertain for thin solid layers where it is possible that  $\text{Al}_3\text{Ti}$  formation is more stable.

---

*Email address:* [a.horsfield@imperial.ac.uk](mailto:a.horsfield@imperial.ac.uk) (Andrew P. Horsfield)

## 1. Introduction

Aluminium alloys are widely used because they are light, strong, resistant to corrosion, and alumina is abundant in the Earth's crust. The mechanical properties of an aluminium component depend on its microstructure, including the average size and shape of the grains, with smaller equiaxed grains generally leading to greater desirable properties such as improved yield strength and toughness due to the Hall-Petch effect [1, 2], together with reduced defects such as porosity[3] and hot tearing [4]. The addition of grain refiners to molten aluminium alloys is known to encourage significant reduction in grain size, and is common industrial practice. However, the mechanism by these grain refiners nucleate  $\alpha$ -Al is still disputed. Therefore, we require a fuller and more detailed understanding of the solidification process, starting with the system under study here: commercial purity (CP) aluminium together with its most commonly used grain refiner, the Al-Ti-B master alloy.

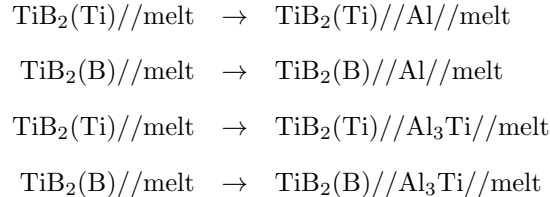
In the decades following the 1950s, grain refiner research focussed on observing results and trends, but did not study the mechanics of the process. However, in the 1990s several transmission electron microscope (TEM) experiments [5, 6, 7, 8, 9, 10] suggested that  $\text{TiB}_2$  was the heterogeneous nucleant responsible for aluminium nucleation, by showing that thin ordered layers of  $\text{Al}_3\text{Ti}$ -like structure (presumed to be  $\text{Al}_3[\text{Ti,Ta}]$ ), had formed off the (0001) face of a  $\text{TiB}_2$  particle in a glass formed from  $\text{Al}_{85}\text{Ni}_{15}\text{Y}_8\text{Co}_2$ . It is, however, unclear what the consequence of using this metallic glass rather than molten CP Al is.

Other experiments showed that, in addition to  $\text{TiB}_2$  particles, excess solute titanium in the melt was also needed for  $\alpha$ -Al nucleation to occur [11]. The role played by this excess Ti is not yet completely understood, but it is thought that in addition to acting as a diffusion restrictor [12], Ti is needed to form  $\text{Al}_3\text{Ti}$  which nucleates off the  $\text{TiB}_2$  forming a thin layer; Al then nucleates off the  $\text{Al}_3\text{Ti}$  layer [13]. The confidence in this  $\text{Al}_3\text{Ti}$  nucleation hypothesis is based on Schumacher's TEM experiments [5, 6, 7, 8, 9, 10], backed up by more recent

TEM experiments by Fan [14], and by in situ synchrotron X-ray diffraction experiments [15], where diffraction peaks corresponding to plane separations similar to the those of bulk  $\text{Al}_3\text{Ti}$  were observed at the onset of aluminium solidification.

35 However, none of these experimental results are able to show the precise chemical composition of the nucleating layer. It is possible that what is being observed in these experiments is actually strained  $\alpha\text{-Al}$ , as suggested by Wang et al. [16], who proposed that the thin layers observed by Schumacher et al. [8] could be strained Al with the same interplanar separation as  $\text{Al}_3\text{Ti}$ . If this is  
40 the true mechanism, then the role of the excess Ti could be to ensure that  $\text{TiB}_2$  particles become Ti-terminated. Other recent static and molecular dynamics calculations using Density Functional Theory (DFT) [17, 16, 18, 19, 20, 21] show that solid Al adheres well to the Ti-terminated face of  $\text{TiB}_2$ , and above the melting point liquid Al shows significant ordering close to this interface,  
45 which suggests it is plausible that Al could nucleate without an  $\text{Al}_3\text{Ti}$  layer. None of these computational studies, however, address the role of excess Ti on the heterogeneous nucleation process.

In this paper, we calculate the total Gibbs energies before and after nucleation, of four hypothetical aluminium nucleation mechanisms:



50 where the two species separated by // denote the characteristic interfaces of the system. The planes parallel to the interfaces are  $\text{TiB}_2(0001)$ , Al (111) and  $\text{Al}_3\text{Ti}$  (112), and the parenthesized element denotes the termination of the  $\text{TiB}_2(0001)$  surface. Using DFT and thermodynamic arguments we address the following questions:

55 1. What are the  $\text{TiB}_2//\text{Al}$  interfacial energies if we account for the effects of

strain within the interfacial plane, and is the strain energy in the interfacial plane significant?

2. What are the  $\text{TiB}_2//\text{Al}_3\text{Ti}$  interfacial energies (also accounting for the effects of interfacial strain) and how do they compare with those of  $\text{TiB}_2//\text{Al}$ ?
- 60 3. Based on the evidence provided both here and in the literature, which of the four nucleation mechanisms is the most favourable?

## 2. Modelling the nucleation of aluminium

Heterogeneous nucleation is the initial formation of a new phase out of an original phase, occurring on a substrate. There are a wide range of methods for  
 65 studying nucleation that are outside the purview of this paper. The interested reader is advised to follow the many good articles cited in this paper, as well as recent books on nucleation, such as that by Greer & Kelton [22]. The total change in Gibbs energy of this process,  $\Delta G_T$ , is defined for an initial system of  
 70  $N_{melt}$  mole-atoms of melt (original phase), transforming into  $N_{solid}$  mole-atoms of solid (new phase) on a substrate, and  $N_{melt'}$  mole-atoms of the remaining unsolidified melt, which might have a slightly different composition to the starting melt. If  $N_{solid}$  is small and completely wets, or wets with a very low contact angle,  $\Delta G_T$  can be approximated by:

$$\Delta G_T = N_{solid}G_{solid} + N_{melt'}G_{melt'} - N_{melt}G_{melt} + \left[ \gamma_{solid}^{melt'} + \gamma_{sub}^{solid} - \gamma_{sub}^{melt} \right] A_{sub} \quad (1)$$

75 where  $G_a$  is the bulk Gibbs energy per mole-atoms of species  $a$ ,  $\gamma_b^a$  is the interfacial energy between species  $a$  and  $b$ , and  $A_{sub}$  is the area of active substrate. For the nucleation reaction considered in this study, the nucleating solid refers to either Al or  $\text{Al}_3\text{Ti}$ , the melt refers to liquid Al with some small amount of dissolved Ti, before (*melt*) and after (*melt'*) the formation of the solid, and the  
 80 substrate refers to the surfaces  $\text{TiB}_2(\text{Ti})$  or  $\text{TiB}_2(\text{B})$ . In this study we are primarily interested in the *difference in*  $\Delta G_T$  between  $\text{Al}_3\text{Ti}$  and Al wetting, given

a particular  $\text{TiB}_2$  substrate, and to see how these differences vary according to  $N_{solid}$ ,  $X_{Ti}$  (or  $\mu_{Ti}$ ), and  $T$  (temperature).

The bulk Gibbs energies will be computed here using formulae from the literature [23, 24, 25, 26, 27], augmented with DFT to include strain effects. The three interfacial energies are determined as follows:  $\gamma_{sub}^{solid}$  is obtained from DFT calculations reported here;  $\gamma_{solid}^{melt'}$  is estimated by interpolating between literature values for similar interfaces where the melt is pure liquid Al and Al-Ti liquid with  $X_{Ti} = 0.0169$  at.%;  $\gamma_{sub}^{melt}$  is estimated through a simple model which involves the surface energies  $\gamma_{sub}^{vac}$  and  $\gamma_{melt}^{vac}$ , calculated using DFT and interpolated literature values respectively. We note that the values of  $N$  and  $A$  are interrelated and depend on assumptions made about the size and shape of the substrate, and of the solid that forms on the substrate.

Note that a central approximation of this paper is the use of static DFT energies – i.e. at 0K, and with no atomic vibrations. Nevertheless it is possible, with our calculated and literature values, to form an approximate expression for  $\Delta G_T$ , especially since our main goal is a *comparison* between different mechanisms.

### 3. Bulk Gibbs Energies

The Gibbs energies of the bulk phases – the  $G$ 's in Eq. 1 – are calculated using the temperature dependent Gibbs energy expressions of the pure elements from the SGTE databases [23], which are empirical equations fitted to the numerous heating and cooling experiments in the literature. To calculate the Gibbs energy of the multi-component phases, the melt (liquid Al with dissolved Ti) and bulk  $\text{Al}_3\text{Ti}$ , the methods and parameters described in Kattner et al. [27] were used. We augment the solid Al and  $\text{Al}_3\text{Ti}$  Gibbs energies with the DFT 0K strain energies from the next section.

Furthermore, the bulk Gibbs energy of the melt is used to obtain the relationship between Ti concentration  $X_{Ti}$  and the chemical potential  $\mu_{Ti}$  using  $\mu_{Ti}^{melt} = \frac{\partial G^{melt}}{\partial N_{Ti}}$ . This enables us to express the interfacial energies as a func-

tion of  $X_{Ti}$ , thereby making all the variables of Eq. 1 functions of the same Ti concentration variable. The chemical potential is a non-linear function of concentration, but locally the activity,  $a_{Ti} = \exp\left(\frac{\mu_{Ti} - \mu_{Ti}^{bulk}}{RT}\right)$ , is approximately linear in  $X_{Ti}$ :  $a_{Ti} = \gamma_{Ti}X_{Ti}$ , where  $\gamma_{Ti}$  (not to be confused with interfacial energy) is the activity coefficient, a dimensionless factor that is a function of  $X_{Ti}$  and temperature. The activity  $\gamma_{Ti}$  is calculated to be about  $2.5 \times 10^{-5} - 3.0 \times 10^{-5}$  around the melting point of Al, at typical melt Ti concentrations of 0.001 to 0.01 at.%, which is broadly in line with that shown by Kostov et al. [28, 29].

## 120 4. Interfacial energies

### 4.1. DFT method

To calculate  $\gamma_{sub}^{solid}$ ,  $\gamma_{sub}^{vac}$  (a term in our  $\gamma_{sub}^{melt}$  model), and the strain energies that make part of  $G_{solid}$ , DFT simulations were performed using the ABINIT code [30, 31, 32], which implements a planewave basis set. A planewave energy cutoff of 30 Ha was used with a PAW [33, 34, 35] auxiliary energy cutoff of 60 Ha. The PBE GGA functional [36] was used for the exchange and correlation energy. Monkhorst-Pack grids [37] of  $6 \times 6 \times 6$  k points for bulk materials, and  $6 \times 6 \times 1$  k points for slabs were employed. Band occupations were calculated using the cold smearing function of Marzari [38]. SCF calculations were converged to within  $10^{-9}$  Ha, while atomic and geometric relaxations were carried out using the BFGS method [39] to within a tolerance of  $5 \times 10^{-5}$  Ha/Bohr per atom for the bulk and surface energy calculations, and  $5 \times 10^{-4}$  Ha/Bohr per atom for the larger, interface calculations. These parameters were chosen after performing extensive convergence tests, to ensure measurable quantities are converged to experimental accuracy: 0.01 J/m<sup>2</sup> for the TiB<sub>2</sub> surface energies, 0.05 J/m<sup>2</sup> for the Al surface energy and TiB<sub>2</sub>//Al interfacial energies, 0.2 J/m<sup>2</sup> for the Al<sub>3</sub>Ti surface energy, and 0.1 J/m<sup>2</sup> for the TiB<sub>2</sub>//Al<sub>3</sub>Ti and interfacial energies; 0.01 for lattice constants.

#### 4.2. Strain effects

140 The solid forming on the substrate ( $\text{TiB}_2(\text{Ti})$  or  $\text{TiB}_2(\text{B})$ ) is assumed to be coherent and dislocation free, based on TEM images [8]. The solid is assumed to stretch to accommodate the strain, since the  $\text{TiB}_2$  substrate is a very large particle (on the atomic scale) of a stiff ceramic [40]; the solid is a thin layer of a less stiff material [41, 42]. Although dislocations will form as the solid becomes  
145 thicker, we are interested only in the region close to the interface i.e. the case when the strained phases are in equilibrium with the liquid and the substrate. Thus while we shall continue to refer to the solid as either Al or  $\text{Al}_3\text{Ti}$ , we shall really mean strained Al or strained  $\text{Al}_3\text{Ti}$ , which ensures that  $\gamma_{sub}^{solid}$  is correctly defined as being independent of the amount of solid. It is shown in section 5  
150 that strain significantly alters the predicted interfacial energy.

#### 4.3. Ti Chemical Potential

In order to calculate the surface and interfacial energies of  $\text{TiB}_2$  by DFT, we require knowledge of the Ti chemical potential,  $\mu_{\text{Ti}}$ , as there is an exchange of Ti between the melt and the nucleated solid, and possibly the substrate.  
155 This chemical potential is sensitive to the Ti concentration in the melt ( $X_{\text{Ti}}$ ). At thermodynamic equilibrium  $\mu_{\text{Ti}}$  should be constant over the entire system; however, as solid forms our system will not be at equilibrium and  $\mu_{\text{Ti}}$  will vary with position. As the Ti reservoir is the Ti in the melt, whose composition remains practically constant, we will take  $\mu_{\text{Ti}}$  to be that for the melt. In the  
160 systems we are studying, there are limitations that restrict the range of  $\mu_{\text{Ti}}$  (and  $X_{\text{Ti}}$ ), which are inferred from the stability of  $\text{TiB}_2$  particles, which do not dissolve in the melt, and the absence of pure Ti or B [43]. Combining the  $\mu_{\text{Ti}}$  and  $\mu_{\text{B}}$  ranges with simple thermodynamic expressions of the formation of  $\text{TiB}_2$ , leads to the expression,  $\Delta G_F^{\text{TiB}_2} < \Delta\mu_{\text{Ti}} < 0$ , where  $\Delta\mu_{\text{Ti}} = \mu_{\text{Ti}} - \mu_{\text{Ti}}^{bulk\text{Ti}}$ , and  
165  $\Delta G_F^{\text{TiB}_2}$  is the Gibbs energy of formation of  $\text{TiB}_2$  (a detailed derivation was done by Han [43]).

#### 4.4. Bulk calculations

A unit cell of each material in its most stable bulk phase at 0K was simulated: fcc for Al; face-centered tetragonal  $DO_{22}$  for  $Al_3Ti$  [44]; hexagonal for  $TiB_2$ ; hcp  
170 for Ti; and a 12-atom rhombohedral cell ( $\alpha$ -phase) for B <sup>1</sup>. The strained bulk states were simulated using 6-layer unit cells of Al(111) and  $Al_3Ti(112)$ , which were allowed to fully relax in the z-direction, but held fixed in the  $x-y$  plane to match the 'a' lattice parameter of  $TiB_2$  ( 3.031 ), thus matching the strained bulk state of Al and  $Al_3Ti$  present in the surface and interfacial slabs presented  
175 in section 4.5.

Table 1 shows the lattice constants obtained from the relaxed bulk simulations, which are later used to define certain cell dimensions in the surface and interface simulations. In addition, the table below shows the calculated energies of bulk formation for  $TiB_2$  and  $Al_3Ti$  (those for Al, Ti and B are zero by  
180 definition), and the strained forms of Al and  $Al_3Ti$ .

The lattice constants agree closely with experiment, with all errors being less than 0.05 , and many being less than 0.01 . The formation energies of relaxed  $TiB_2$  and  $Al_3Ti$  are also close to the experimental values. Table 1 shows that strained Al and  $Al_3Ti$  have significantly higher energies than their relaxed counterparts, and that the strain induced on the solid to match the  $TiB_2$  substrate  
185 is greater for  $Al_3Ti$  than for Al: their bulk strain energies are:  $\Delta G_{strain}^{Al} = +2.2$  kJ/mol-atoms and  $\Delta G_{strain}^{Al_3Ti} = +16$  kJ/mol-atoms. This significant difference in strain energy is likely caused by  $Al_3Ti$  having a tetragonal structure rather than a regular fcc one like Al, which has two important consequences: firstly,  
190 the first  $Al_3Ti$  (112) plane, unlike Al (111), does not exactly align with the perfect hexagonal structure of  $TiB_2(0001)$ ; secondly, whilst the Al (111) planes are

---

<sup>1</sup> $\alpha$ -B is not quite the B ground state, but it is used because it is much simpler than the real ground state, the  $\beta$ -phase ( $\sim 105$  atoms per unit cell) whilst the difference in energy per atom between  $\alpha$ -B and  $\beta$ -B is very small. Recent DFT calculations [45] found the difference in energy per atom between  $\alpha$ -B and  $\beta$ -B to be only 0.29 kJ/mol, which would make less than 0.01 J/m<sup>2</sup> difference to the final interfacial energies.

Phase	Lattice constant (Å)		Formation energy (kJ/mol)	
	calculated	experimental	calculated relaxed/strained	experimental relaxed
Al	a = 4.051	a = 4.0496 [46]	0/+2.2	-
Ti	a = 2.933 c = 4.657	a = 2.9506 [46] c = 4.6835	0	-
B	a = 5.049	a = 5.064 [47]	0	-
Al <sub>3</sub> Ti	a = 3.853 c = 8.632	a = 3.8537 [48] c = 8.5839	-155/-90	-150 [44]
TiB <sub>2</sub>	a = 3.0314 c = 3.2228	a = 3.0236 [40] c = 3.2204	-310	-322 [49]

Table 1: The lattice constants and formation energies obtained from bulk calculations at 0 K and prior experiments.

vertically aligned, repeating every three planes, the Al<sub>3</sub>Ti (112) planes lean at about 5 degrees from the vertical. Subsequently, fixing the Al<sub>3</sub>Ti (112) planes to conform to TiB<sub>2</sub>(0001) results in compression of some of the atoms in the plane and extra induced strain to straighten the slab.

It is important to note that by using 0K strain energies we have neglected differences in the strain that might arise due to thermal expansion and compositional disorder [27], instead assuming the ideal lattice occupancies in the DFT cells. The 0K strain energies will be used with the temperature-dependent relaxed bulk energies for Al and Al<sub>3</sub>Ti derived in section 3. This should not significantly affect the main results, since the experimentally determined lattice expansion coefficients for Al and TiB<sub>2</sub> [50, 40] and the theoretically determined values for Al<sub>3</sub>Ti [51] show that going from 0K to the melting temperature of Al would result in fairly small reductions in lattice mismatch for both Al (111) (~ +5.5% to +4.2%) and Al<sub>3</sub>Ti (112) (~ +11.2% to +10.7% and +4.7% to +4.6%). Furthermore, the Al mismatch, already lower than the Al<sub>3</sub>Ti mismatch at 0K, is reduced by a greater amount at the Al melting point, hence the main result of this paper, that TiB<sub>2</sub>(Ti)//Al is the favoured nucleation mechanism, would

likely be reinforced if thermal expansion was taken into account.

210 *4.5. Surface and interfacial energy calculations*

The following single material surface slabs were simulated: Al(111), strained Al(111), Al<sub>3</sub>Ti(112), strained Al<sub>3</sub>Ti(112), TiB<sub>2</sub>(Ti), and TiB<sub>2</sub>(B). The supercells for TiB<sub>2</sub>(Ti) and TiB<sub>2</sub>(B) were seven layer slabs, containing 10 and 11 atoms respectively (the same as simulated by Han [43]), while the Al and Al<sub>3</sub>Ti  
215 supercells were six layer slabs, containing 6 and 24 atoms respectively (the Al<sub>3</sub>Ti supercells contain 4 atoms per layer, as each layer must have 1 Ti atom for every 3 Al atoms). The strained Al and Al<sub>3</sub>Ti supercells differ from their relaxed counterparts by having the cell parameters in the plane of the interfaces fixed to match those of the TiB<sub>2</sub> slabs.

220 Four interfacial supercells were simulated, each a slab containing seven layers of TiB<sub>2</sub> adhered to six layers of strained solid, Al (111) or Al<sub>3</sub>Ti (112). Hence a 16 atom TiB<sub>2</sub>(Ti)//Al, a 17 atom TiB<sub>2</sub>(B)//Al, a 64 atom TiB<sub>2</sub>(Ti)//Al, and a 68 atom TiB<sub>2</sub>(B)//Al<sub>3</sub>Ti supercell were simulated.

The vacuum added to each surface and interface supercell was least 13 Å  
225 thick, sufficient to prevent interaction between periodic images. The number of layers of each material was tested for convergence to ensure a good representation of the bulk material, while still remaining small enough for a full accuracy run: seven layers of TiB<sub>2</sub>, six layers of Al, six layers of Al<sub>3</sub>Ti, and six Al layers' worth of vacuum were found to converge  $\gamma$  to 0.05 J/m<sup>2</sup> for TiB<sub>2</sub>//Al and 0.2  
230 J/m<sup>2</sup> for TiB<sub>2</sub>//Al<sub>3</sub>Ti (these are conservative estimates), while the difference in  $\gamma$  between systems, which is more important, converged even more tightly.

The surface and interfacial energies are calculated by the common method of subtracting away appropriate amounts of bulk energy, dividing by the area, and then, for interface systems, subtracting any excess surface energy[52] . For  
235 example, the interfacial energy calculated from the TiB<sub>2</sub>(Ti)//Al slab is:

$$\gamma_{TiB_2(Ti)}^{Al} = \frac{1}{A} (E^{slab} - \{3\mu_{TiB_2}^{bulk} + \mu_{Ti}^{slab} + 6\mu_{Al}^{bulk}\}) - \{\gamma_{TiB_2(Ti)}^{vac} + \gamma_{Al}^{vac}\}2)$$

The  $\mu_{Ti}$  term is needed because the TiB<sub>2</sub>(Ti) substrate in the supercell does not

Solid surface	Relaxed $\sigma$ ( $\text{Jm}^{-2}$ )		Strained $\sigma$ ( $\text{Jm}^{-2}$ )
	This work	Previous work	This work
Al (111)	0.82	0.939[53]	0.96
Al <sub>3</sub> Ti (112)	0.97	0.92[54]	1.08

Table 2: Relaxed and strained surface energies of the solid, Al and Al<sub>3</sub>Ti, calculated from our slab simulations, compared with other simulation results.

contain a whole number of TiB<sub>2</sub> units (this is discussed in Han’s TiB<sub>2</sub> surface study [43]). Thus  $\gamma$  for all systems involving a TiB<sub>2</sub> substrate are functions of  $\mu_{Ti}$ , and are thus expressed as a range, going from minimum  $\mu_{Ti}$  to maximum  $\mu_{Ti}$ .

#### 4.6. Surface and interfacial energy results

The surface energies of TiB<sub>2</sub>,  $\gamma_{TiB_2(Ti)}^{vac}$  and  $\gamma_{TiB_2(B)}^{vac}$ , were calculated to be 5.47 – 2.23 J/m<sup>2</sup> and 2.99 – 6.23 J/m<sup>2</sup> respectively, which is in very close agreement with Han’s results [43]. The surface energies of relaxed and strained Al and Al<sub>3</sub>Ti are shown in table 2.

It is interesting to note that, although the surface energy of strained Al is less than that of strained Al<sub>3</sub>Ti, (strained to achieve coherency with a TiB<sub>2</sub> substrate that is), compared to its relaxed counterpart, the strain seems to have a greater comparative effect on Al than on Al<sub>3</sub>Ti, which is the reverse trend to what was seen for the bulk energy discussed in the previous section.

Our calculated interfacial energies are shown in table 3, and plotted in figure 1 (the plot treats the strained bulk as the reference system). Note that the negative values of interfacial energies shown in these tables and graphs are actually unphysical, but we have kept them to help the reader fully see and compare each plot.

Our values for TiB<sub>2</sub>(Ti)//Al and TiB<sub>2</sub>(B)//Al are in close agreement with those from previous simulations [17], while there are no published interface calculations for the Al<sub>3</sub>Ti systems that we are aware of. As explained in section 2, the use of the strained bulk energies to calculate the interfacial energy makes

System	$\gamma$ (J/m <sup>2</sup> )		
	Previous work	This work (inc. <i>xy</i> strain)	This work (exc. <i>xy</i> strain)
TiB <sub>2</sub> (Ti)//Al	3.25 – -0.08[17]	3.04 – -0.20	2.62 – -0.62
TiB <sub>2</sub> (B)//Al	1.12 – 4.45 [17]	0.99 – 4.23	0.57 – 3.82
TiB <sub>2</sub> (Ti)//Al <sub>3</sub> Ti	-	3.61 – 0.37	2.93 – -0.31
TiB <sub>2</sub> (B)//Al <sub>3</sub> Ti	-	0.46 – 3.71	-0.21 – 3.03

Table 3: Calculated ranges of values for the interfacial energies - the first number in the range is for  $\mu_{Ti} = -0.12$  Ha/atom. (-310 kJ/mol-a.); the second number is for  $\mu_{Ti} = 0$  Ha/atom (0 kJ/mol-a.).

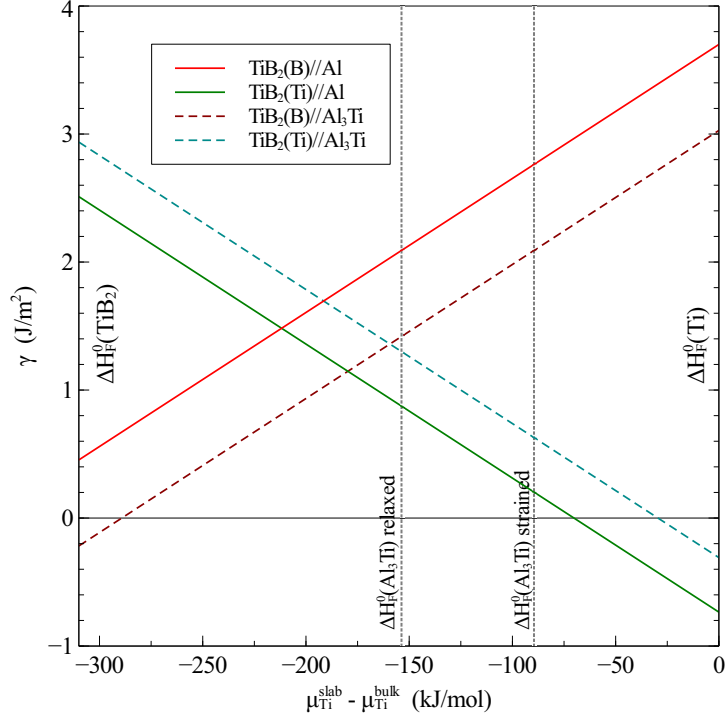


Figure 1: Interfacial energy versus Ti chemical potential for the four interfacial systems. The energies of formation of Al<sub>3</sub>Ti, both relaxed and strained, are shown by the vertical dotted lines.

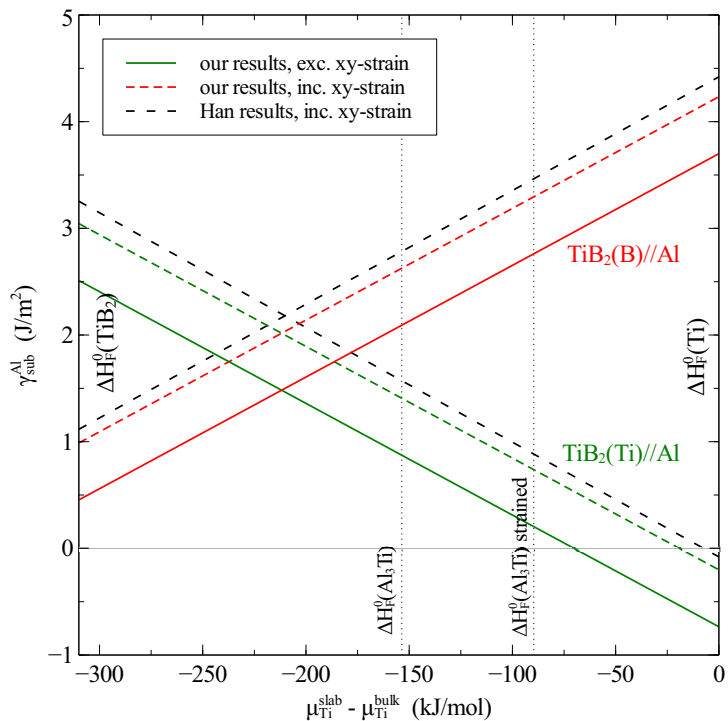


Figure 2: Interfacial energies of  $\text{TiB}_2//\text{Al}$  for the present results – both with and without  $x$ - $y$  strain – and Han’s results [17], which include  $x$ - $y$  strain.

260 a significant difference to the results, which figure 2 demonstrates. The small  
 difference between our strain-included  $\gamma$  and those of Han may be at least partly  
 explained by Han’s use of ultrasoft pseudopotentials, in contrast to our use of  
 PAW.

The results from figure 1 suggest three main findings concerning  $\gamma_{sub}^{solid}$ :

- 265
1. Both solid Al and  $\text{Al}_3\text{Ti}$  form a more stable interface with  $\text{TiB}_2(\text{Ti})$  than  
 $\text{TiB}_2(\text{B})$  at higher Ti chemical potentials; at lower Ti chemical potentials,  
 $\text{TiB}_2(\text{B})$  forms the more stable interface.
  2. The  $\text{TiB}_2(\text{Ti})$  substrate forms more stable interfaces with Al than with  
 $\text{Al}_3\text{Ti}$ ; conversely,  $\text{TiB}_2(\text{B})$  forms more stable interfaces with  $\text{Al}_3\text{Ti}$  than  
 270 Al.
  3. We see that for higher Ti concentrations ( $\Delta\mu_{\text{Ti}} \gtrsim -184$  kJ/mol, which

around the melting point equates to  $X_{Ti} \gtrsim 0.0003\text{at.}\%$ ) the most stable interface is  $\text{TiB}_2(\text{Ti})//\text{Al}$ ; for lower Ti concentrations ( $\Delta\mu_{Ti} \lesssim -184 \text{ kJ/mol}$  or  $X_{Ti} \lesssim 0.0003\text{at.}\%$ ) the most stable is  $\text{TiB}_2(\text{B})//\text{Al}_3\text{Ti}$ . However, bulk  $\text{Al}_3\text{Ti}$  is not stable in this range, but only stable when  $\Delta\mu_{Ti} > -90 \text{ kJ/mol}$ .

It therefore seems that based on the GS substrate//solid interfacial energies alone,  $\text{TiB}_2(\text{Ti})//\text{Al}$  is the most favorable system.

#### 4.7. Solid-liquid interfacial energies

We now consider the solid-liquid interfacial energies  $\gamma_{sub}^{melt}$  and  $\gamma_{solid}^{melt}$ . The  $\gamma_{solid}^{melt}$  values,  $\gamma_{Al}^{melt}$  and  $\gamma_{Al_3Ti}^{melt}$ , are estimated as follows:  $\gamma_{Al}^{melt}$  at 660K was taken as a linear interpolation between literature values of  $\gamma_{Al}^{Al(l)}$  (0.131 J/m<sup>2</sup> – the average of 0.121 J/m<sup>2</sup> [55] and 0.141 J/m<sup>2</sup> [56]) and  $\gamma_{Al}^{melt(X_{Ti}=0.0169\%)}$  (rounded up to 0.171 J/m<sup>2</sup> [57]). The effect of strain – we are actually dealing with  $\gamma_{Al-strained}^{melt}$  – was estimated by calculating the difference that straining Al makes to the Al(111)//vacuum surface energy,  $\{\sigma_{Al-strained}^{vac} - \sigma_{Al-relaxed}^{vac}\}$ , and was found to be 0.258 J/m<sup>2</sup> (see table 2). This results in an estimate for  $\gamma_{Al}^{melt}$  of 0.389 J/m<sup>2</sup>. For  $\gamma_{Al_3Ti}^{melt}$ , a similar method was used, except that the two values to interpolate between were themselves estimated, due to a lack of literature values, using  $\gamma_{Al_3Ti}^{Al(l)} \approx \gamma_{Al}^{Al(l)} + (\gamma_{TiB_2(Ti)}^{Al_3Ti} - \gamma_{TiB_2(Ti)}^{Al})$  and  $\gamma_{Al_3Ti}^{melt(X_{Ti}=0.0169\%)} \approx \gamma_{Al}^{melt(X_{Ti}=0.0169\%)} + (\gamma_{TiB_2(Ti)}^{Al_3Ti} - \gamma_{TiB_2(Ti)}^{Al})$ .

*Modelling  $\gamma_{sub}^{melt}$ .* To estimate the interfacial energy between the melt and the substrate we have built a simple model. We start by expressing  $\gamma_{sub}^{melt}$  as follows:

$$\gamma_{sub}^{melt} = \gamma_{sub}^{vac} + \gamma_{melt}^{vac} + \Delta\gamma_{sub}^{melt} \quad (3)$$

where  $\Delta\gamma_{sub}^{melt}$  is the difference in total interfacial and surface energies caused by the immersion of the substrate into the melt. For  $\gamma_{sub}^{vac}$  we use the 0K interfacial energies obtained from the DFT surface energy calculations (see table 2). For  $\gamma_{melt}^{vac}$  we start with  $\gamma_{Al(liq)}^{vac}$  as 1 J/m<sup>2</sup> [58, 59, 60] and use the same linear interpolation as for  $\gamma_{solid}^{melt}$  above, and then add the 0K difference between the

strained and relaxed solid Al surface energies, which is 0.14 J/m<sup>2</sup> (see table 2).  
 300 The energy changes caused by  $\Delta\gamma_{sub}^{melt}$  are based only on the amount of ordering  
 of the liquid at the substrate, based on the results of DFT MD simulations by  
 Wang [16] and Zhang [18, 21]. An ordering function is used,  $a(z)$ , to quantify  
 the state of the liquid at a distance  $z$  from the substrate (0 is perfect disorder,  
 i.e. liquid; 1 is perfect order, i.e. solid), and is approximated by an exponential  
 305 function,  $a(z) = \exp(-kz)$  where  $k$  is a disordering parameter. Based on Wang's  
 [16] diagrams of the nuclei's final positions and the density profile away from  
 the interface,  $k$  was set to  $0.25 \times 10^{-10} \text{ m}^{-1}$  and  $1 \times 10^{-10} \text{ m}^{-1}$  for TiB<sub>2</sub>(B)  
 and TiB<sub>2</sub>(Ti). The interfacial free energy is then computed using the procedure  
 detailed in the supplementary material, and is a function of  $a(z)$ , and thus  
 310 ultimately a function of  $k$ . Our final expression for  $\gamma_{sub}^{melt}$  is:

$$\gamma_{sub}^{melt} = \gamma_{sub}^{vac} + \gamma_{melt}^{vac} - b\rho_{liq} \left( \frac{8}{3} \frac{\rho_{liq}}{\Delta\rho} + \frac{1}{4} \right) k^{-1} \quad (4)$$

where  $b$  is the temperature dependent Gibbs energy of fusion of the Al liquid,  
 $\rho_{liq}$  is the density of Al liquid, and  $\Delta\rho = \rho_{solid} - \rho_{liq}$  with  $\rho_{solid}$  being the density  
 of the solid. While very simple, this model contains two important elements:  
 firstly, the interfacial energy varies with respect to  $X_{Ti}$ , because  $\gamma_{sub}^{vac}$  and  $\gamma_{melt}^{vac}$   
 315 vary with  $X_{Ti}$ ; secondly, it contains an element,  $\Delta\gamma_{sub}^{melt}$ , that lowers  $\gamma_{sub}^{melt}$  in  
 proportion to the amount of ordering seen at the substrate i.e. more ordering,  
 means a lower  $\gamma_{sub}^{melt}$ . Figure 3 shows the interfacial energy derived from the  
 model using the values of  $k$  given above.

The plots for  $\gamma_{sub}^{melt}$  are quite similar to those of  $\gamma_{sub}^{solid}$  (and  $\gamma_{sub}^{vac}$ ), but shifted  
 320 about 3.5 – 4 J/m<sup>2</sup> (1 J/m<sup>2</sup>) higher. The crossover point occurs at about  
 $\mu_{Ti} = -200 \text{ kJ/mol}$ , which around the melting point of Al corresponds to  $X_{Ti} =$   
 $1 \times 10^{-7}$  to  $1 \times 10^{-6}$ . In a typical industrial melt  $X_{Ti}$  is about  $1 \times 10^{-5}$  to  $1 \times 10^{-4}$ ,  
 hence TiB<sub>2</sub>(Ti) is predicted to be the more stable substrate prior to nucleation,  
 and hence, the two nucleation mechanisms starting with TiB<sub>2</sub>(Ti)//melt appear  
 325 to be the most likely nucleation mechanisms. However, the possibility that  
 TiB<sub>2</sub>(B) substrates might still be present is discussed in the analysis section.

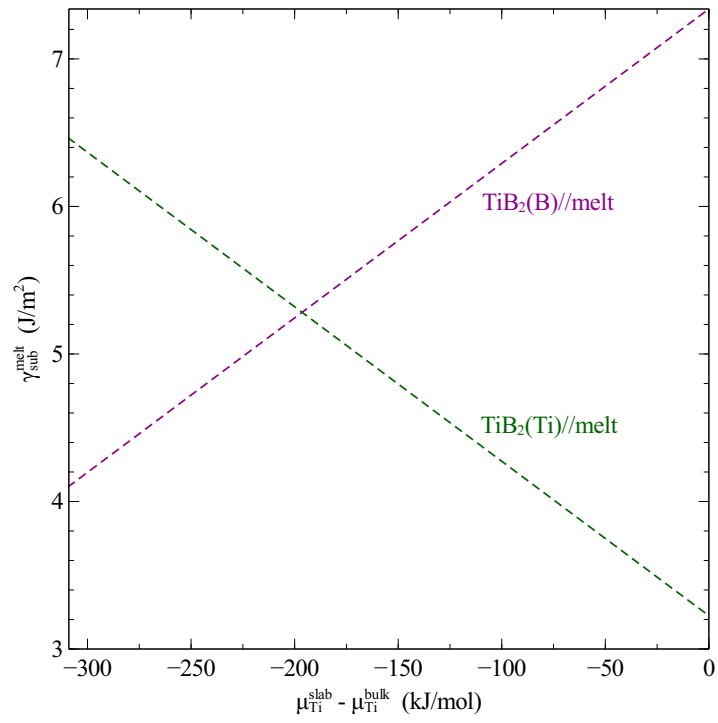


Figure 3: The interfacial energy between TiB<sub>2</sub> substrates and the melt,  $\gamma_{sub}^{melt}$ , plotted against  $\mu_{Ti} - \mu_{Ti}^{bulk}$ , according to our model .

#### 4.8. Finite temperature corrections to interfacial energy

One major limitation of the  $\gamma_{sub}^{solid}$  and  $\gamma_{sub}^{melt}$  figures is that they were calculated using GS DFT simulations, and so do not include finite temperature effects. Further DFT perturbation calculations (DFPT), implementing the harmonic approximation, can be used to estimate the finite temperature effects. However, at the temperatures considered here (close to the melting point), the harmonic approximation breaks down and further anharmonic effects need to be considered, which would be very computationally demanding and beyond the scope of this paper. However, some preliminary DFPT calculations using an LDA exchange correlation functional and norm-conserving pseudopotentials were carried out to see qualitatively how the finite temperature corrections affect the initial substrate//melt system and the  $\Delta G_T$  for the nucleation of Al. These preliminary results suggest that the final conclusion, which predicts the TiB<sub>2</sub>(Ti)//Al nucleation mechanism as the most favoured, would not be affected by the finite temperature corrections. Please see the supplementary material for more details. For this study, the GS results shown in sections 4 and 4.7 are used for the  $\Delta G_T$  analysis in section 5.

### 5. $\Delta G_T$ Analysis

The interfacial energies from section 4 and the bulk energies from section 3 are now inserted into Eq. 1 to calculate the total Gibbs energy of solid formation, and analyse it as a function of solid thickness  $n$ , Ti concentration  $X_{Ti}$ , and temperature  $T$ . It must be emphasised that this analysis does not say anything about the critical point of nucleation, that is, the most stable number of layers of solid. According to Eq. 1, above the melting point and even slightly below it, one layer of solid should be the most stable arrangement, because the first layer reduces the overall Gibbs energy by reducing the total interfacial energy, while the formation of further layers of solid would only increase the total Gibbs energy, because the formation of strained solid, Al or Al<sub>3</sub>Ti, is positive (see table 1). Yet Eq. 1 is derived from macroscopic equilibrium thermodynamics,

and it is unclear how closely very thin layers of solid obey these rules. Hence, the analysis will consider separately a thin layer system (1 atomic layer) and a thick layer system (6 atomic layers), in order to more clearly identify where any uncertainty in the conclusions lies.

360 We make assumptions about the size, shape, and number density of  $\text{TiB}_2$  substrates, based on estimates by Greer [61]: the average diameter of the substrate =  $3\mu\text{m}$ , the particle density =  $1 \times 10^{14}$  particles/ $\text{m}^2$ , and the fraction of active particles = 0.001. This gives a total active substrate area =  $4.93 \times 10^{-7}\text{m}^2/\text{mol-atoms}$  of melt. The value of these constants does significantly influence the absolute values of  $G_T$  and  $\Delta G_T$ , but they have a negligible effect on the difference in  $\Delta G_T$  between the 4 systems. Throughout, unless specified otherwise,  $X_{T_i}$  is taken to be fixed at a typical value of  $5 \times 10^{-5}$  mole fraction (0.01wt%) used in industry, and the temperature is taken to be 950K, which is approximately when wetting on the substrate is first observed [15].

### 370 5.1. $G_T$ and $\Delta G_T$ vs $n$ layers

Figure 4 shows the absolute values of  $G_T$  plotted against the number of layers  $n$ . We see that under typical melt conditions,  $\text{TiB}_2(\text{Ti})//\text{melt}$  is the most stable starting system before nucleation, and  $\text{TiB}_2(\text{Ti})//\text{Al}//\text{melt}$  is the most stable after nucleation. Hence this plot supports  $\text{TiB}_2(\text{Ti})//\text{melt} \rightarrow$  375  $\text{TiB}_2(\text{Ti})//\text{Al}//\text{melt}$  as the most likely nucleation mechanism. Interestingly, if the starting system is  $\text{TiB}_2(\text{B})//\text{melt}$ , it is much less clear whether  $\text{TiB}_2(\text{B})//\text{Al}//\text{melt}$  or  $\text{TiB}_2(\text{B})//\text{Al}_3\text{Ti}//\text{melt}$  would be the most stable system after nucleation. The evidence above suggests that thin layers of solid  $\text{Al}_3\text{Ti}$  might be more stable than thin layers of solid Al, on a  $\text{TiB}_2(\text{B})$  substrate.

380 Figure 5 shows the difference in values of  $\Delta G_T$ , the Gibbs energy change due to nucleation, plotted as functions of  $n$ , the number of layers of solid. It shows the most likely solid, Al or  $\text{Al}_3\text{Ti}$ , given a particular starting substrate - a negative value indicates that solid Al formation is more stable, whereas a positive value indicates that solid  $\text{Al}_3\text{Ti}$  formation is more stable. There is a clear trend that as  $n$  increases, formation of Al becomes more and more 385

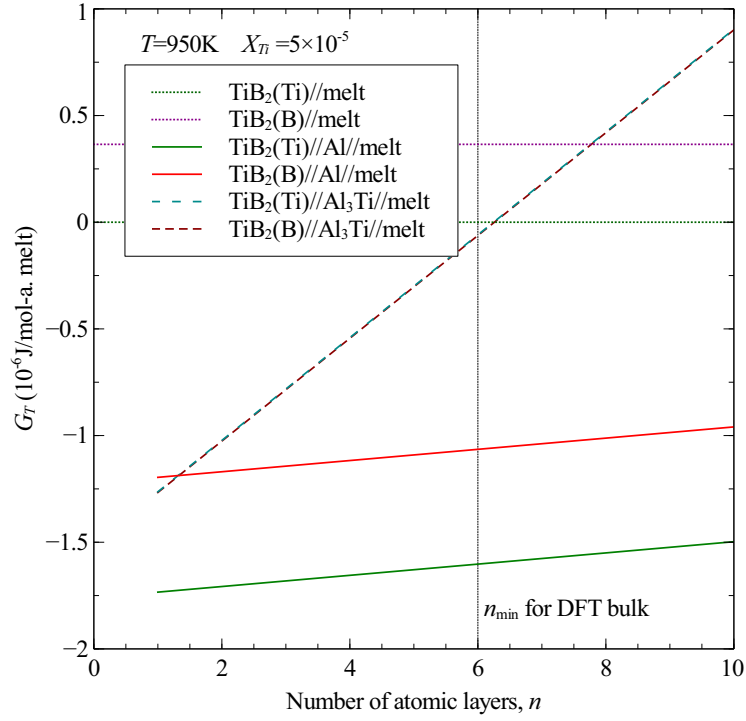


Figure 4: The total Gibbs energy,  $G_T$ , of the initial and final systems. The absolute value of  $G_T$  is arbitrary: here the value for the initial  $\text{TiB}_2(\text{Ti})//\text{melt}$  system is chosen as zero. *Note:* the  $\text{TiB}_2(\text{Ti})//\text{Al}_3\text{Ti}//\text{melt}$  and  $\text{TiB}_2(\text{B})//\text{Al}_3\text{Ti}//\text{melt}$  lines are very similar and are overlapping on this plot.

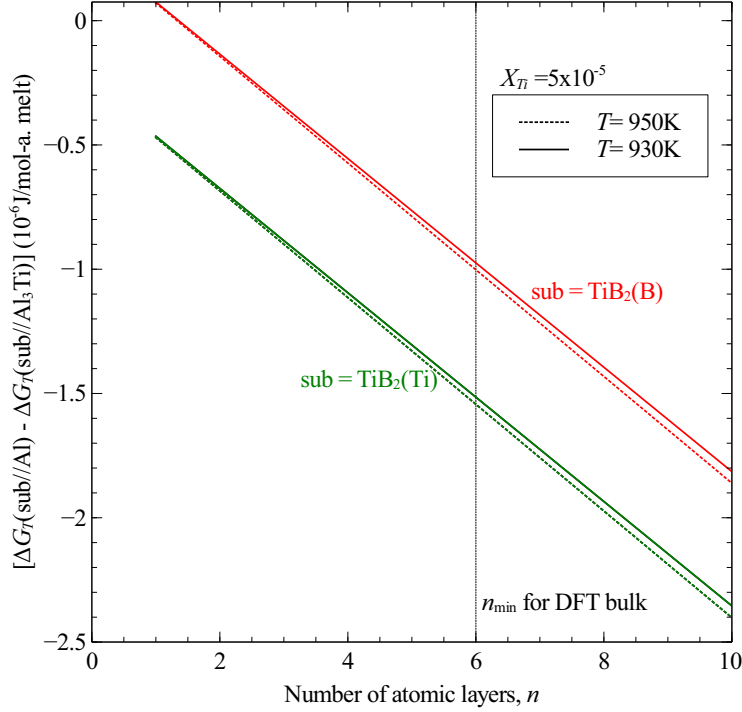


Figure 5: The difference in  $\Delta G_T$  between formation of  $n$  layers of Al and  $\text{Al}_3\text{Ti}$ , for both substrates, at two different temperatures. The vertical line in both graphs represents the minimum number of layers of solid beyond which subsequent layers are bulk-like, according to our DFT calculations.

favourable over  $\text{Al}_3\text{Ti}$ .

### 5.2. $\Delta G_T$ vs $X_{\text{Ti}}$ and $T$

Figure 6 shows the effects of varying  $X_{\text{Ti}}$  and  $T$ , for thin and thick layers of solid. As expected from the Al-Ti phase diagram, an increase in  $X_{\text{Ti}}$  increases the stability of  $\text{Al}_3\text{Ti}$  relative to Al. In the range of  $X_{\text{Ti}}$  shown here, which is typical of an industrial aluminium melt, and for much higher  $X_{\text{Ti}}$ , the Al-favouring trends shown in figure 5 do not change – that is, for 6 atomic layers on  $\text{TiB}_2(\text{B})$ , and any amount of solid thickness on  $\text{TiB}_2(\text{Ti})$ , it remains that Al is much more stable than  $\text{Al}_3\text{Ti}$ . However, for thin layers of solid forming on  $\text{TiB}_2(\text{B})$ ,  $\text{Al}_3\text{Ti}$  appears to be more stable, although there is significant un-

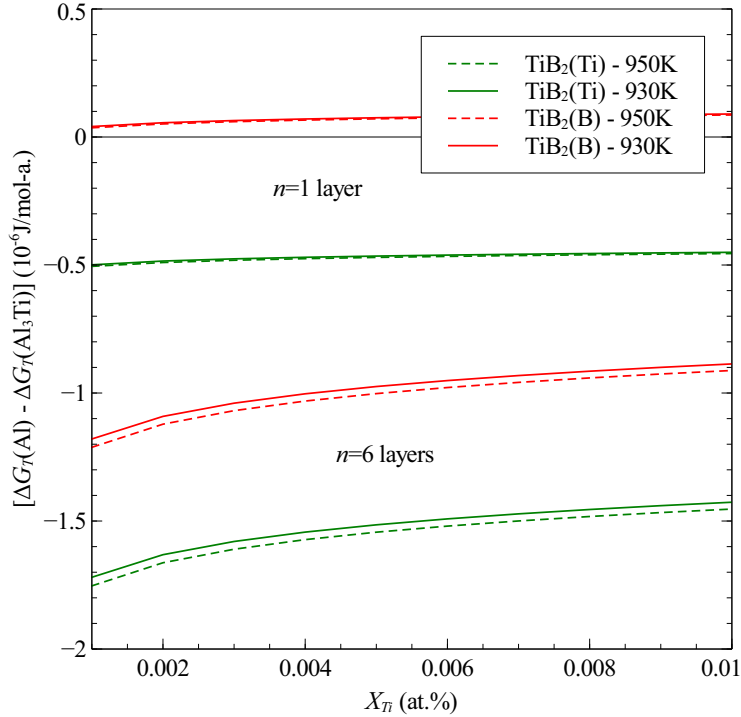


Figure 6: The difference in  $\Delta G_T$  for the formation of 1 and 6 layers of Al and  $\text{Al}_3\text{Ti}$  on both substrates, plotted against  $X_{Ti}$ , at two different temperatures.

certainty in which solid is more stable. It is quite possible that the cross-over point – below which thin layers of  $\text{Al}_3\text{Ti}$  would cease to be more stable than thin layers of Al – might lie within an industrially relevant composition. Direct evidence for the  $\text{TiB}_2(\text{B})//\text{Al}_3\text{Ti}$  mechanism was not seen in Wang’s DFT  
400 MD simulation, but it is possible that a longer simulation with more Ti atoms in the liquid at the  $\text{TiB}_2(\text{B})$  surface might show at least one  $\text{Al}_3\text{Ti}$  layer form spontaneously at the surface. The effect of decreasing temperature decreases slightly the likelihood of Al forming: this effect becomes more noticeable for thicker amounts of solid.

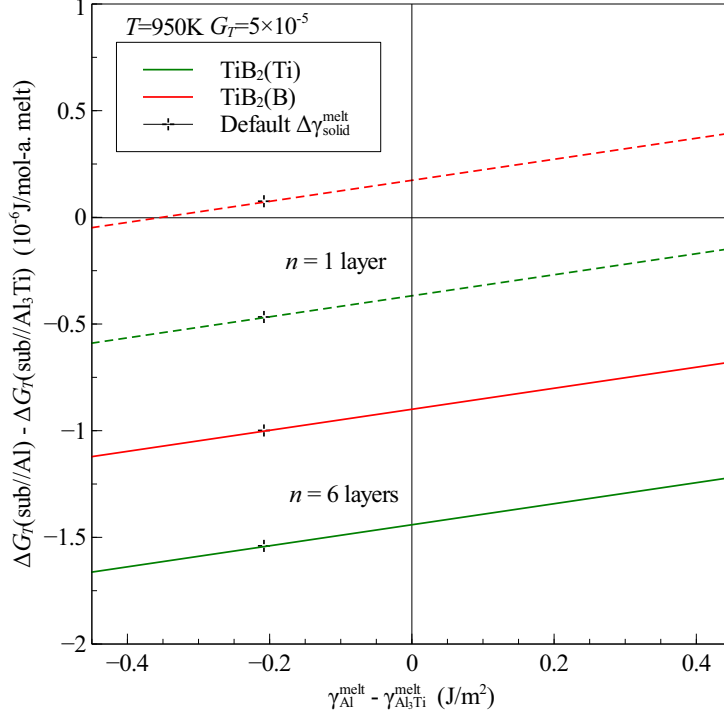


Figure 7: Plot of the difference in  $\Delta G_T$  between sub//Al and sub//Al<sub>3</sub>Ti mechanisms against  $\gamma_{\text{Al}}^{\text{melt}} - \gamma_{\text{Al}_3\text{Ti}}^{\text{melt}}$ . The left half of the graph represents cases where (strained) Al has a lower interfacial energy with the melt than does Al<sub>3</sub>Ti; vice versa for the right half of the graph.

### 405 5.3. $\Delta G_T$ sensitivity to $\gamma^{\text{melt}}$ values

This and the next subsection look at how sensitive the  $\Delta G_T$  results are to the  $\gamma^{\text{melt}}$  values, which were calculated relatively roughly compared to the  $G$  and  $\gamma_{\text{sub}}^{\text{solid}}$  values. Figure 7 shows the effects of varying the estimates for  $\gamma_{\text{solid}}^{\text{melt}}$ , specifically the difference  $\gamma_{\text{Al}}^{\text{melt}} - \gamma_{\text{Al}_3\text{Ti}}^{\text{melt}}$ . The plot shows that for both

410 thick and thin layers of solid on a  $\text{TiB}_2(\text{Ti})$  substrate, quite large variations in  $\gamma_{\text{Al}}^{\text{melt}} - \gamma_{\text{Al}_3\text{Ti}}^{\text{melt}}$  from the value we used ( $-0.208 \text{ J/m}^2$ , shown by the crosses) would not alter the original conclusion that thick layers of Al are more stable than Al<sub>3</sub>Ti on both  $\text{TiB}_2$  substrates. However, for thin layers on a  $\text{TiB}_2(\text{B})$  substrate, the more stable solid is reasonably sensitive to variations in  $\gamma_{\text{Al}}^{\text{melt}} - \gamma_{\text{Al}_3\text{Ti}}^{\text{melt}}$  – a

415 shift to  $-0.35 \text{ J/m}^2$  would make Al more stable than Al<sub>3</sub>Ti.

Figure 8 looks at the effect of varying the solid//liquid interfacial energy of our starting system,  $\gamma_{sub}^{melt}$ , specifically  $\gamma_{TiB_2(Ti)}^{melt} - \gamma_{TiB_2(B)}^{melt}$ . Previous graphs have plotted the  $\Delta G_T$  difference between Al and Al<sub>3</sub>Ti mechanisms, *given a particular substrate* - that is the more useful comparison if we assume that in our

420 real system all or almost all of the substrates have the same termination. However, we may wish to consider the possibility that both substrates are available in the melt. In this case, we would want to know, *given a particular nucleating solid*, what is the more favourable substrate, and this is what figure 8 shows. The plot suggests that the precise value of  $\gamma_{TiB_2(Ti)}^{melt} - \gamma_{TiB_2(B)}^{melt}$  is important in

425 determining the favoured substrate. It is very likely, given our values for  $\gamma_{TiB_2}^{Al(s)}$  and  $\gamma_{TiB_2}^{vac}$ , that  $\gamma_{TiB_2(Ti)}^{melt} - \gamma_{TiB_2(B)}^{melt}$  is also negative in typical industrial  $X_{Ti}$  and  $T$ . Our default results confirm that Al nucleation clearly favours TiB<sub>2</sub>(Ti) as a substrate, and Al<sub>3</sub>Ti nucleation favours TiB<sub>2</sub>(B). These results are fairly stable with respect to errors in our  $\gamma_{TiB_2(Ti)}^{melt} - \gamma_{TiB_2(B)}^{melt}$  estimation. However,

430  $\gamma_{sub}^{melt}$  was estimated using the ordering of liquid Al atoms only, and not Al atoms with some dissolved Ti. Understanding how the presence of Ti atoms affects this ordering is an interesting topic of ongoing research [21].

## 6. Conclusions

Four potential mechanisms for the nucleation of aluminium were investigated and compared. Four interfaces were simulated using DFT, each involving

435 a substrate, TiB<sub>2</sub>(Ti) or TiB<sub>2</sub>(B), and a nucleated solid, Al or Al<sub>3</sub>Ti. Each interfacial energy was calculated as a function of the Ti chemical potential, itself a function of Ti concentration ( $X_{Ti}$ ) and temperature ( $T$ ) in the melt. The interfacial energy was then combined with Gibbs energy data from the literature

440 to assess the nucleating potential of each mechanism. The following conclusions are made:

1. Regarding the stability of the interfaces at 0K: the TiB<sub>2</sub>(Ti)//Al interface is more stable than TiB<sub>2</sub>(Ti)//Al<sub>3</sub>Ti for all values of  $X_{Ti}$ ; the TiB<sub>2</sub>(B)//Al<sub>3</sub>Ti interface is more stable than TiB<sub>2</sub>(B)//Al for all values

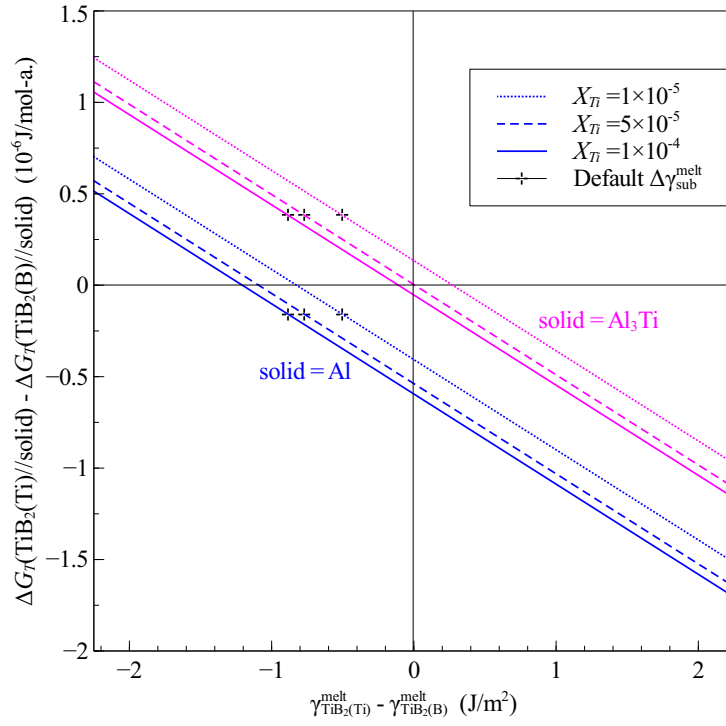


Figure 8: The difference in  $\Delta G_T$  between formation of a solid on  $\text{TiB}_2(\text{Ti})$  and  $\text{TiB}_2(\text{B})$ , plotted against the difference in the starting solid-liquid interfacial energy  $\gamma_{\text{TiB}_2(\text{Ti})}^{\text{melt}} - \gamma_{\text{TiB}_2(\text{B})}^{\text{melt}}$ . The left half of the graph represents cases where  $\text{TiB}_2(\text{Ti})$  has the lower interfacial energy with the melt; the right half likewise for  $\text{TiB}_2(\text{B})$ . This difference in  $\Delta G_T$  is plotted for each solid separately, at  $T=950\text{K}$ , for three different  $X_{\text{Ti}}$ .

445 of  $X_{Ti}$ ; the most stable interface at 0K is  $TiB_2(Ti)//Al$  for  $X_{Ti} \gtrsim 0.0003$   
at.%, and  $TiB_2(B)//Al_3Ti$  for  $X_{Ti} \lesssim 0.0003$  at.%. Strain plays a signifi-  
cant role in the value of the interfacial energy, adding about  $0.5 \text{ J/m}^2$  to  
 $TiB_2//Al$  interfacial energies.

2. The results here suggest that any possible  $Al_3Ti$  layers that do form, on  
450 either substrate, are likely to be very thin, and probably significantly  
thinner than any Al layers that might form.
3.  $TiB_2(Ti)$  is more stable in the melt than  $TiB_2(B)$  prior to nucleation. In  
this case, formation of Al is more stable than  $Al_3Ti$  formation, for thin  
and thick solid layers. However, if  $TiB_2(B)$  is present in the melt prior to  
455 nucleation, then only for thick solid layers is formation of Al is more stable  
over  $Al_3Ti$ , whilst for thin solid layers, it is unclear whether formation of  
Al or  $Al_3Ti$  is more stable, but our results slightly favour  $Al_3Ti$ .

The results and analysis as they stand point towards a mechanism wherein  
either something similar to pure Al, rather than  $Al_3Ti$ , nucleates off a  $TiB_2(Ti)$   
460 substrate, or else a mixture of Al and  $Al_3Ti$ , perhaps an intermediate Al-Ti  
structure, nucleates off a  $TiB_2(B)$  substrate. Given the non-uniform and locally  
varying nature of real-life interfaces, it is a possibility that any combination of  
these mechanisms are active at once throughout the melt. One thing all the  
suggested mechanisms have in common, however, is Ti contact with both B and  
465 Al, whether in the last Ti layer of  $TiB_2$ , or in the first layer of  $Al_3Ti$ .

To get closer to a firm conclusion several extensions to this work could be  
made. Firstly, the liquid-solid interfacial energies, which were modelled quite  
simply in this study, need to be calculated accurately as a function of  $X_{Ti}$  and  
 $T$ . Secondly, all interfacial energies, which were fully or partially calculated at  
470 0 K in this study, should be calculated at finite temperature. Finally, while  
the classical model has been useful to observe general trends between the four  
systems, in response to several parameters, ultimately large scale long running  
DFT MD calculations of  $TiB_2$  substrates in the presence of liquid melt need to  
be run.

475 **Acknowledgements**

The authors would like to acknowledge financial support from ESPRC (grant numbers EP/I02249X/1 and GR/T26344/1), and further financial support from the ExoMet Project (which is co-funded by the European Commission in the 7th Framework Programme (contract FP7-NMP3-LA-2012- 280421), by the European Space Agency and by the individual partner organisations), and the Research Complex at Harwell. The authors would like to further acknowledge the use of the CX1 high performance computer at Imperial College London, and thank Simon Burbidge for his invaluable help and advice on CX1, and Junsheng Wang for his previous work which lead to this current study. This work was made possible by the facilities and support provided by the Diamond-Manchester Collaboration and the Research Complex at Harwell, funded in part by the EPSRC (EP/I02249X/1).

- [1] E. O. Hall, The deformation and ageing of mild steel: Iii discussion of results, Proceedings of the Physical Society. Section B 64 (9) (1951) 747.
- 490 [2] N. J. Petch, The cleavage strength of polycrystals, Engineering Technology & Applied Sciences (19) (1982) 24–24.
- [3] P. Lee, A. Chirazi, D. See, Modeling microporosity in aluminum-silicon alloys: a review, Journal of Light Metals 1 (1) (2001) 15 – 30.
- [4] D. G. Eskin, Suyitno, L. Katgerman, Mechanical properties in the semi-solid state and hot tearing of aluminium alloys, Progress In Materials Science 49 (5) (2004) 629–711.
- 495 [5] P. Schumacher, A. L. Greer, Devitrification behavior of the stable al-rich amorphous alloy  $\text{Al}_{85}\text{Ni}_5\text{Y}_8\text{Co}_2$ , Amorphous Metallic Materials 81-3 (1993) 631–636.
- 500 [6] P. Schumacher, A. L. Greer, Heterogeneously nucleated  $\alpha$ -Al in amorphous aluminum-alloys, Materials Science and Engineering A 178 (1-2) (1994) 309–313.

- [7] P. Schumacher, A. L. Greer, Studies of the action of grain-refining particles in aluminium alloys, *Light Metals* 1995 (1995) 869–877.
- 505 [8] P. Schumacher, A. L. Greer, High-resolution transmission electron microscopy of grain-refining particles in amorphous aluminium alloys, *Light Metals* 1996 (1996) 745–753.
- [9] P. Schumacher, A. L. Greer, On the reproducibility of heterogeneous nucleation in amorphous  $\text{Al}_{85}\text{Ni}_{10}\text{Ce}_5$  alloys, *Materials Science and Engineering A-structural Materials Properties Microstructure and Processing* 226  
510 (1997) 794–798.
- [10] P. Schumacher, A. L. Greer, J. Worth, P. V. Evans, M. A. Kearns, P. Fisher, A. H. Green, New studies of nucleation mechanisms in aluminium alloys: implications for grain refinement practice, *Materials Science and Technology* 14 (5) (1998) 394–404.  
515
- [11] P. S. Mohanty, F. H. Samuel, J. E. Gruzleski, Studies on addition of inclusions to molten aluminum using a novel technique, *Metallurgical and Materials Transactions B* 26 (1) (1995) 103–109.
- [12] A. Prasad, L. Yuan, P. D. Lee, D. H. StJohn, The interdependence model of grain nucleation: A numerical analysis of the nucleation-free zone, *Acta Materialia* 61 (16) (2013) 5914–5927.  
520
- [13] B. S. Murty, S. A. Kori, M. Chakraborty, Grain refinement of aluminium and its alloys by heterogeneous nucleation and alloying, *International Materials Reviews* 47 (1) (2002) 3–29.
- 525 [14] Z. Fan, Y. Wang, Y. Zhang, T. Qin, X. R. Zhou, G. E. Thompson, T. Pennycook, T. Hashimoto, Grain refining mechanism in the al/al-ti-b system, *Acta Materialia* 84 (2015) 292–304.
- [15] N. Iqbal, N. H. van Dijk, S. E. Offerman, N. Geerlofs, M. P. Moret, L. Katgerman, G. J. Kearley, In situ investigation of the crystallization kinetics

- 530 and the mechanism of grain refinement in aluminum alloys, *Materials Science and Engineering A* 416 (1-2) (2006) 18–32.
- [16] J. S. Wang, A. Horsfield, U. Schwingenschlogl, P. D. Lee, Heterogeneous nucleation of solid al from the melt by  $\text{TiB}_2$  and  $\text{Al}_3\text{Ti}$ : An ab initio molecular dynamics study, *Physical Review B* 82 (18) (2010) 184203.
- 535 [17] Y. F. Han, Y. B. Dai, D. Shu, J. Wang, B. D. Sun, First-principles calculations on the stability of Al/TiB<sub>2</sub> interface, *Applied Physics Letters* 89 (14).
- [18] H. L. Zhang, Y. F. Han, Y. B. Dai, J. Wang, B. D. Sun, An ab initio molecular dynamics study: liquid-Al/solid-TiB<sub>2</sub> interfacial structure during heterogeneous nucleation, *Journal of Physics D-applied Physics* 45 (45)  
540 (2012) 455307.
- [19] H. L. Zhang, Y. F. Han, J. Wang, Y. B. Dai, B. D. Sun, An ab initio molecular dynamics study on the structural and electronic properties of  $\text{AlB}_2$ ,  $\text{TiB}_2$  and  $(\text{Al-x, Ti}(1-x))\text{B}_2$  in al-ti-b master alloys, *Journal of Alloys and Compounds* 585 (2014) 529–534.  
545
- [20] H. L. Zhang, Y. F. Han, Y. B. Dai, S. S. Lu, J. Wang, J. Zhang, D. Shu, B. D. Sun, An ab initio study on the electronic structures of the solid/liquid interface between  $\text{TiB}_2$  (0001) surface and al melts, *Journal of Alloys and Compounds* 615 (2014) 863–867.
- 550 [21] H. L. Zhang, Y. F. Han, W. Zhou, Y. B. Dai, J. Wang, B. D. Sun, Atomic study on the ordered structure in al melts induced by liquid/substrate interface with ti solute, *Applied Physics Letters* 106 (4) (2015) 041606.
- [22] K. Kelton, A. L. Greer, *Nucleation in Condensed Matter*, Elsevier, 2010.
- [23] A. T. Dinsdale, SGTE Data For Pure Elements, *CALPHAD: Computer Coupling of Phase Diagrams and Thermochemistry-* 15 (4) (1991) 317–425.  
555

- [24] O. Kubaschewski, W. Dench, The heats of formation in the systems titanium-aluminium and titanium-iron, *Acta Metallurgica* 3 (4) (1955) 339 – 346.
- [25] R. Pretorius, R. Dereus, A. M. Vredenberg, F. W. Saris, Use of the effective  
560 heat of formation rule for predicting phase formation sequence in Al-Ni systems, *Materials Letters* 9 (12) (1990) 494–499.
- [26] M. Sujata, S. Bhargava, S. Sangal, On the formation of  $\text{TiAl}_3$  during reaction between solid Ti and liquid Al, *Journal of Materials Science Letters* 16 (14) (1997) 1175–1178.
- [27] U. R. Kattner, J. C. Lin, Y. A. Chang, Thermodynamic assessment and  
565 calculation of the Ti-Al system, *Metallurgical Transactions A-physical Metallurgy and Materials Science* 23 (8) (1992) 2081–2090.
- [28] A. Kostov, B. Friedrich, D. Zivkovic, Thermodynamic calculations in alloys Ti-Al, Ti-Fe, Al-Fe and Ti-Al-Fe, *Journal of Mining and Metallurgy Section*  
570 *B-metallurgy* 44 (1) (2008) 49–61.
- [29] A. Kostov, D. Zivkovic, Thermodynamic analysis of alloys Ti-Al, Ti-V, Al-V and Ti-Al-V, *Journal of Alloys and Compounds* 460 (1-2) (2008) 164–171.
- [30] ABINIT code, a common project of the Universite Catholique de Louvain, Corning Incorporated, and other contributors (URL:  
575 <http://www.abinit.org>).
- [31] X. Gonze, G. M. Rignanese, M. Verstraete, J. M. Beuken, Y. Pouillon, R. Caracas, F. Jollet, M. Torrent, G. Zerah, M. Mikami, P. Ghosez, M. Veithen, J. Y. Raty, V. Olevano, F. Bruneval, L. Reining, R. Godby, G. Onida, D. R. Hamann, D. C. Allan, A brief introduction to the ABINIT software  
580 package, *Zeitschrift F ur Kristallographie* 220 (5-6) (2005) 558–562.
- [32] X. Gonze, B. Amadon, P. M. Anglade, J. . M. Beuken, F. Bottin, P. Boulanger, F. Bruneval, D. Caliste, R. Caracas, M. Cote, T. Deutsch,

- 585 L. Genovese, P. Ghosez, M. Giantomassi, S. Goedecker, D. R. Hamann,  
P. Hermet, F. Jollet, G. Jomard, S. Leroux, M. Mancini, S. Mazevet,  
M. J. T. Oliveira, G. Onida, Y. Pouillon, T. Rangel, G. M. Rignanese,  
D. Sangalli, R. Shaltaf, M. Torrent, M. J. Verstraete, G. Zerah, J. W.  
Zwanziger, ABINIT: First-principles approach to material and nanosystem  
properties, *Computer Physics Communications* 180 (12) (2009) 2582–2615.
- [33] N. Holzwarth, pAW atomic data for element Al - generated by AtomPAW  
590 (N. Holzwarth) + AtomPAW2Abinit v3.1.1.
- [34] N. Holzwarth, pAW atomic data for element B - Generated by AtomPAW  
(N. Holzwarth)+ AtomPAW2Abinit v3.2.1.
- [35] D. Vanderbilt, titanium PAW data extracted from US-*psp* (D.Vanderbilt)  
- generated by US*pp2*Abinit v2.3.0.
- 595 [36] J. P. Perdew, K. Burke, M. Ernzerhof, Generalized gradient approximation  
made simple, *Physical Review Letters* 77 (18) (1996) 3865–3868.
- [37] H. J. Monkhorst, J. D. Pack, Special points for brillouin-zone integrations,  
*Physical Review B* 13 (12) (1976) 5188–5192.
- [38] N. Marzari, Ab-initio molecular dynamics for metallic systems, Ph.D. the-  
600 sis, University of Cambridge (1996).
- [39] T. H. Fischer, J. Almlof, General-methods for geometry and wave-function  
optimization, *Journal of Physical Chemistry* 96 (24) (1992) 9768–9774.
- [40] R. G. Munro, Material properties of titanium diboride, *Journal of Research  
of the National Institute of Standards and Technology* 105 (5) (2000) 709–  
605 720.
- [41] W. X. Li, T. C. Wang, Ab initio investigation of the elasticity and stability  
of aluminium, *Journal of Physics-condensed Matter* 10 (43) (1998) 9889–  
9904.

- [42] C. L. Fu, Electronic, elastic, and fracture properties of trialuminide alloys  
610 -  $\text{Al}_3\text{Sc}$  and  $\text{Al}_3\text{Ti}$ , *Journal of Materials Research* 5 (5) (1990) 971–979.
- [43] Y. F. Han, Y. B. Dai, D. Shu, J. Wang, B. D. Sun, First-principles study of  
 $\text{TiB}_2(0001)$  surfaces, *Journal of Physics: Condensed Matter* 18 (17) (2006)  
4197–4205.
- [44] C. Colinet, A. Pasturel, Structural stability of one-dimensional long-period  
615 structures in the  $\text{TiAl}_3$  compound, *Journal of Physics-condensed Matter*  
14 (26) (2002) 6713–6727.
- [45] M. J. van Setten, M. A. A. Uijttewaai, G. A. de Wijs, R. A. de Groot,  
Thermodynamic stability of boron: The role of defects and zero point mo-  
tion, *Journal of the American Chemical Society* 129 (9) (2007) 2458–2465,  
620 pMID: 17295480.
- [46] W. M. E. Haynes, *CRC Handbook of Chemistry and Physics*, 92nd ed.,  
CRC, 2011.
- [47] G. Will, B. Kiefer, Electron deformation density in rhombohedral alpha-  
boron, *Zeitschrift Fur Anorganische Und Allgemeine Chemie* 627 (9) (2001)  
625 2100–2104.
- [48] P. Norby, A. N. Christensen, Preparation and Structure of  $\text{Al}_3\text{Ti}$ , *Acta*  
*Chemica Scandinavica Series A-physical and Inorganic Chemistry* 40 (2)  
(1986) 157–159.
- [49] A. Jain, R. Pankajavalli, S. Anthonysamy, K. Ananthasivan, R. Babu,  
630 V. Ganesan, G. S. Gupta, Determination of the thermodynamic stability  
of  $\text{TiB}_2$ , *Journal of Alloys and Compounds* 491 (1-2) (2010) 747–752.
- [50] F. C. Nix, D. MacNair, The thermal expansion of pure metals: Copper,  
gold, aluminum, nickel, and iron, *Phys. Rev.* 60 (1941) 597–605.
- [51] S. Saha, T. Z. Todorova, J. W. Zwanziger, Temperature dependent lattice  
635 misfit and coherency of  $\text{al}_3\text{x}$  ( $\text{x} = \text{sc}$ ,  $\text{zr}$ ,  $\text{ti}$  and  $\text{nb}$ ) particles in an  $\text{al}$  matrix,  
*Acta Materialia* 89 (2015) 109–115.

- [52] W. Zhang, J. R. Smith, Stoichiometry and adhesion of nb/al(2)o(3), Physical Review B 61 (24) (2000) 16883–16889.
- [53] J. Schochlin, K. Bohnen, K. Ho, Structure and dynamics at the Al(111)-  
640 surface, Surface Science 324 (1995) 113 – 121.
- [54] J. Wang, A. Horsfield, P. D. Lee, P. Brommer, Heterogeneous nucleation of solid al from the melt by al<sub>3</sub>ti: Molecular dynamics simulations, Physical Review B 82 (14) (2010) 144203.
- [55] R. H. Ewing, Free-energy of crystal-melt interface from radial distribution  
645 function - further calculations, Philosophical Magazine 25 (4) (1972) 779–784.
- [56] Y. Waseda, W. A. Miller, Calculation of crystal-melt interfacial free-energy from experimental radial-distribution function data, Transactions of the Japan Institute of Metals 19 (10) (1978) 546–552.
- 650 [57] K. Keslioglu, M. Gunduz, H. Kaya, E. Cadirli, Solid-liquid interfacial energy in the Al-Ti system, Materials Letters 58 (24) (2004) 3067–3073.
- [58] J. M. Molina, R. Voytovych, E. Louis, N. Eustathopoulos, The surface tension of liquid aluminium in high vacuum: The role of surface condition, International Journal of Adhesion and Adhesives 27 (5) (2007) 394–401.
- 655 [59] I. Egry, J. Brillo, D. Holland-Moritz, Y. Plevachuk, The surface tension of liquid aluminium-based alloys, Materials Science and Engineering A-structural Materials Properties Microstructure and Processing 495 (1-2).
- [60] H. Kobatake, J. Brillo, J. Schmitz, P.-Y. Pichon, Surface tension of binary al-si liquid alloys, Journal of Materials Science 50 (9) (2015) 3351–3360.
- 660 [61] A. L. Greer, Grain refinement of alloys by inoculation of melts, Philosophical Transactions of the Royal Society A-mathematical Physical and Engineering Sciences 361 (1804) (2003) 479–494.

## Highlights

$\text{TiB}_2(\text{Ti})//\text{Al}$  interfacial energy is significantly reduced when  $xy$  strain is removed.

$\text{TiB}_2(\text{Ti})//\text{Al}_3\text{Ti}$  interfacial energies are calculated for the first time.

On the  $\text{TiB}_2(\text{Ti})$  substrate, Al forms a more stable interface than  $\text{Al}_3\text{Ti}$ .

On the  $\text{TiB}_2(\text{B})$  substrate, thin layers of  $\text{Al}_3\text{Ti}$  form a more stable interface than Al.

Aluminium nucleation is proposed to occur directly off Ti-terminated  $\text{TiB}_2$ .

**Supplementary Material for on-line publication only**

**[Click here to download Supplementary Material for on-line publication only: SupplInfo.pdf](#)**

**LaTeX Source Files**

[Click here to download LaTeX Source Files: latex.zip](#)